Hindawi
International Journal of Agronomy
Volume 2018, Article ID 7935140, 13 pages
https://doi.org/10.1155/2018/7935140

Research Article

Application of the Flux-Variance Technique for Evapotranspiration Estimates in Three Types of Agricultural Structures

Ori Ahiman,[1] Yonatan Mekhmandarov,[1] Moran Pirkner,[1] and Josef Tanny[1,2]

[1]*Institute of Soil, Water and Environmental Sciences, Agricultural Research Organization, The Volcani Center, P.O. Box 15159, Rishon LeZion 7528809, Israel*
[2]*HIT-Holon Institute of Technology, P.O. Box 305, Holon 58102, Israel*

Correspondence should be addressed to Josef Tanny; tanai@volcani.agri.gov.il

Received 21 December 2017; Revised 27 March 2018; Accepted 4 April 2018; Published 11 June 2018

Academic Editor: Paolo Inglese

Irrigation of protected crops requires sound knowledge of evapotranspiration. Previous studies have established that the eddy-covariance (EC) technique is suitable for whole canopy evapotranspiration measurements in large agricultural screenhouses. Nevertheless, the eddy-covariance technique remains difficult to apply in the farm due to costs, operational complexity, and postprocessing of data, thereby inviting alternative techniques to be developed. The subject of this paper is the evaluation of a turbulent transport technique, the flux variance (FV), whose instrumentation needs and operational demands are not as elaborate as the EC, to estimate evapotranspiration within large agricultural structures. Measurements were carried out in three types of agricultural structures: (i) a banana plantation in a light-shading (8%) screenhouse (S1), (ii) a pepper crop in an insect-proof (50-mesh) screenhouse (S2), and (iii) a tomato crop in a naturally ventilated greenhouse with a plastic roof and 50-mesh screened sidewalls (S3). Quality control analysis of the EC data showed that turbulence development and flow stationarity conditions in the three structures were suitable for flux measurements. However, within the insect-proof screenhouse (below the screen) and the plastic-covered greenhouse, R^2 of the energy balance closure was poor; hence, the alternative simple method could not be used. Results showed that the FV technique was suitable for reliable estimates of ET in shading and insect-proof screenhouses with R^2 of the regressions between FV latent heat flux and latent heat flux deduced from energy balance closure of 0.99 and 0.92 during validation for S1 and S2, respectively.

1. Introduction

In recent years, the area of vegetables and orchards grown in protected cultivation systems is constantly increasing. These include, among other structures, naturally ventilated greenhouses [1], insect-proof screenhouses [2], and shading screenhouses [3]. These structures are naturally ventilated and hence have significant interaction with the external environment. The advantages and limitations of such protected cultivation systems are well documented in the literature [4, 5].

Protected crops are exposed to microclimatic conditions that are significantly different from those in the open field. Hence, the interaction between protected crops and their microenvironment has been the topic of much research during the past years (e.g., [6–8]). One effect of covering the crops is in modifying the exchange of energy, mass, and momentum between the plants and their environment. This modification may affect the evapotranspiration; that is, the water vapor flux from the canopy to the atmosphere, which, in turn, will affect the irrigation demands. The possibility of water saving through reduced transpiration and irrigation demands initiated a number of research studies focused on evapotranspiration measurements and estimates, mainly in screenhouses [3, 9–13].

The most common method for direct measurements of evapotranspiration and other scalar fluxes is the eddy covariance [14]. The method was originally developed and

mostly used for flux measurements over open surfaces like forests, natural, or agricultural fields and open water bodies. Due to its high capabilities in reliable measurements of whole canopy evapotranspiration, in recent years, its performance was also examined in protected environments like screenhouses.

Results obtained in various screenhouses [2, 3, 9, 12, 13] illustrated the reliability of the eddy-covariance technique within such protected environments. In all these studies, the EC system was deployed above the plants and below the screen, at a height which is smaller than twice the canopy height. Although conditions at such a height apparently do not meet the common requirements for flux measurements [15], turbulence analysis and flux results supported the use of the EC method at such heights within screenhouses. For example, Tanny et al. [3] evaluated the suitability of the eddy-covariance technique to directly measure evapotranspiration in a large banana screenhouse with almost mature plants. Results were promising: they found 94% closure of the energy balance and daily evapotranspiration values, in agreement with the irrigation applied by the grower. Even though their EC system was deployed relatively close to the canopy top, the spectral energy density decayed with the frequency in a rate close to −5/3, suggesting that turbulence properties resembled the flow in the inertial subrange of steady-boundary layers. Tanny et al. [12] extended these results by measuring turbulent fluxes simultaneously with two EC systems installed at two heights above the crop and below the screen within a large banana screenhouse. Similar friction velocities were measured at the two levels, validating the constant-flux layer assumption within the air gap between the canopy top and the horizontal screen.

Due to the high cost of sensors and complex operation and data analysis, the EC method is inaccessible for day-to-day use by growers as a tool for irrigation management. To assist growers in improving irrigation management, a family of simplified methods was developed in recent years that are capable of indirectly estimating the canopy sensible heat flux and extracting evapotranspiration as a residual of the energy balance closure. One method of this family is the flux-variance (FV) method, which is derived from the MOST principle that any scalar variance normalized by the scalar flux depends on atmospheric stability only. Using this theory, it can be shown that, under unstable conditions, the sensible heat flux is proportional to $\sigma_T^{3/2}$, where σ_T is the standard deviation of air temperature measured at high frequency (~10 Hz) above the canopy. Hence, the method can be applied using fast response single-point measurement of air temperature [16] and auxiliary, relatively simple measurements of net radiation and soil heat flux.

The flux-variance (FV) method, which is the topic of the present paper, has been applied in several studies in open fields. There are three technical aspects involved with applying the FV method: measurement height, sampling frequency, and the available fetch. *Measurement height*: no study in the literature identified the optimal height where the measurement of sensible heat flux, H, is in best agreement with a reference value. Most literature studies show measurements that were done at a single height in the surface layer, larger than 1.1 h_c (e.g., [16]), that is, within and above the roughness sublayer which is about 2 h_c. *Measurement frequency*: most studies reported sampling frequencies between 0.1 and 20 Hz [17–19]; however, no report compared the method's performance at different frequencies to identify the optimal one. *Fetch*: literature studies were conducted under height/fetch ratio in the range 1 : 90–1 : 200 [17, 18, 20].

Several studies examined the value of C_T, the similarity constant associated with the FV method (see Section 2) and the correlation between EC and FV sensible heat fluxes. The value of C_T was in the range 0.9–1.1, and the coefficient of correlation with EC sensible heat flux was in the range 0.72–0.98 [17–20].

The main goal of the present study was to examine the FV technique for crops cultivated in three modified environments that are very common in regions of mild winter climates like the Mediterranean basin [4]. The structures examined are a tomato greenhouse with impermeable plastic roof and screened sidewall openings for natural ventilation, an insect-proof screenhouses with dense net that blocks insect invasion, in which pepper was grown, and a banana screenhouse that protects the crop from hail, high wind speed, and supraoptimal solar radiation. The ultimate goal is to provide guidelines on the optimal use of the FV technique in estimating ET for irrigation management in such structures. Hence, sensible heat flux estimates using FV are used for extracting evapotranspiration from the energy balance closure, and results are compared with ET measurements.

2. Theory

The detailed theory of the flux-variance method is given by Wesson et al. [16]. This section provides only a brief outline with major equations.

The Monin-Obukhov similarity theory (MOST) implies that any nondimensional turbulence statistics depends on the atmospheric stability only, $\zeta = (z - d)/L$, where z is the measurement height, d is the zero-plane displacement height, and L is the Obukhov length defined as follows:

$$L = -\frac{u_*^3 T}{kg\langle w'T'\rangle}, \tag{1}$$

where $u_* = (\langle u'w'\rangle^2 + \langle v'w'\rangle^2)^{1/4}$ is the friction velocity, u', v', and w' are fluctuations in longitudinal, transversal, and vertical velocity components, respectively, T is air temperature, k is von-Karman's constant, g is the gravitational acceleration, and $\langle w'T'\rangle$ is the covariance between vertical velocity and temperature fluctuations which represents the mean kinematic sensible heat flux. Based on MOST, the air temperature standard deviation can be expressed as follows:

$$\frac{\sigma_T}{T_*} = f(-\zeta), \tag{2}$$

where T_* is the temperature scaling parameter given by $T_* = \langle w'T'\rangle/u_*$. As shown by Albertson et al. [21] and

Wesson et al. [16] under unstable conditions, the temperature standard deviation, σ_T, can be approximated by the following equation:

$$\frac{\sigma_T}{T_*} = C_T(-\zeta)^{-1/3}, \quad (3)$$

where $C_T = 0.99$ is a similarity constant [22]. From (2) and (3), it can be shown that

$$H_{\mathrm{FV}} = \rho c_{\mathrm{p}} \langle w'T' \rangle = \rho c_{\mathrm{p}} \left(\frac{\sigma_T}{C_T}\right)^{3/2} \left(\frac{kg(z-d)}{T}\right)^{1/2}, \quad (4)$$

where ρ is the air density and c_{p} is the air specific heat at constant pressure. Hence, the sensible heat flux can be estimated by calculating the temperature standard deviation obtained from a single-point measurement of air temperature at high-sampling frequency. Note that (4) can only predict positive sensible heat fluxes under unstable conditions since $\sigma_T \geq 0$. An approximate expression for stable conditions was also suggested [16], but analysis of such conditions was outside the scope of the present study.

To estimate evapotranspiration, the energy balance closure equation is used as $LE + H = Rn - G$, where LE is the latent heat flux (evapotranspiration), H is the sensible heat flux, Rn is the net radiation, and G is the soil heat flux. The FV latent heat flux is extracted by $LE_{\mathrm{FV}} = Rn - G - H_{\mathrm{FV}}$, where H_{FV} is the flux variance sensible heat flux calculated by (4). Since in the present study, the measured energy balance was not perfectly closed (see Section 4), a "closed" LE_{EB} was estimated, derived by forcing the energy balance closure [23] using the eddy-covariance sensible heat flux, $LE_{\mathrm{EB}} = Rn - G - H_{\mathrm{EC}}$. Finally, the flux-variance latent heat flux, LE_{FV}, is validated against the "closed" latent heat flux, LE_{EB}.

3. Materials and Methods

3.1. Sites, Crops, and Structures. The study is based on three comprehensive field campaigns carried out in three different agricultural structures each with a different crop. Details on each of the campaigns are given below (see also [24] for details on S1 and S2).

3.1.1. Campaign S1: Banana, 8% Shading Screen. The screenhouse was located at 32°42′N; 34°57′E, 20 m AMSL, on the Mediterranean coastline in western Israel near the Carmel mountain. The calibration period was 7.08.2011–29.08.2011 (DOY 219–241), during which 21 days were analyzed. Screenhouse dimensions were $250 \times 450\,\mathrm{m}^2$ and 5.5 ± 0.1 m high, with the longer side oriented nearly east-west (Figure 1). Screenhouse cover was a woven screen, with nominal shading of 8% (manufacturer's data), and a rectangular hole of 2.3 mm × 3 mm, made of clear, round polyethylene monofilaments 0.3 mm in diameter (Polysack Plastic Industries Inc., Israel). Banana, *Grand Nain* AAA, was planted during May 2011, in groups of four, separated 4.5 m between rows and 3.5 m between plants in a row. During the experiment, plant height was 4.3 m and Leaf area index (LAI) was 1.4. Plants were irrigated following regional recommendations for screenhouse banana. Soil comprised 44% clay, 26% sand, and 30% silt. Dry and volumetric soil heat capacities were $C_{\mathrm{d}} = 0.86\ \mathrm{J \cdot g^{-1} \cdot K^{-1}}$ and $C_{\mathrm{V}} = 1.57\ \mathrm{MJ \cdot m^{-3} \cdot K^{-1}}$ [25].

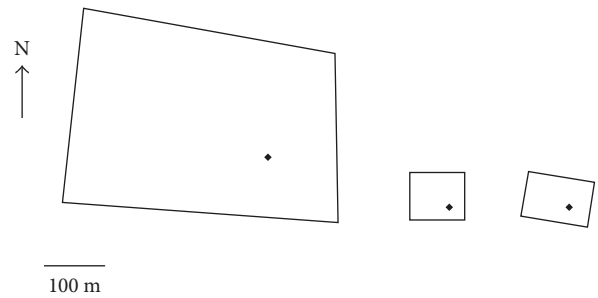

Figure 1: A schematic top-view of the three structures examined. The diamond symbol represents the location of the eddy-covariance and flux-variance sensors. From left to right: S1, banana screenhouse; S2, pepper screenhouse; S3, tomato greenhouse.

3.1.2. Campaign S2: Pepper, 50-Mesh Insect-Proof Screenhouse. The screenhouse was located at 31°48′N; 35°28′E, −380 m AMSL, in the Jordan Valley of eastern Israel. The calibration period was 13.05.2013–15.06.2013 (DOY 133–166), during which 34 days were analyzed. Screenhouse dimensions were $100 \times 110\,\mathrm{m}^2$ and 3.8 ± 0.1 m in height, with the longer side oriented east-west (Figure 1). Screenhouse was covered by a white insect-proof 50-mesh screen woven of round polyethylene monofilaments, 0.23 mm in diameter, with hole size of 0.46 mm (Ginegar Inc., Israel). Pepper 1715 (Hish-Till, Inc. Israel) was planted on the 15th of September 2012, upon rows 0.60 m wide, separated 1 m apart, with plant density of $3.5\ \mathrm{plants \cdot m^{-2}}$. During measurements, plant height was constant at 1.6 ± 0.1 m. Plants were planted in compost channels, which were dug into the local Reg soil, and irrigated following regional recommendations. The Reg soil comprised 50% clay, 25% sand, and 25% silt. The compost comprised 90% clay, 5% sand, and 5% silt [26]. Thus, the dry and volumetric soil heat capacities were $C_{\mathrm{d}} = 0.9\ \mathrm{J \cdot g^{-1} \cdot K^{-1}}$ and $C_{\mathrm{V}} = 1.72\ \mathrm{MJ \cdot m^{-3} \cdot K^{-1}}$ [25].

3.1.3. Campaign S3: Tomato, Naturally Ventilated Greenhouse. The greenhouse was located at 31°44′N; 35°27′E, −400 m AMSL in the western shore of the Dead Sea, near Kibbutz Kalia. The calibration period was 20.01.2014–23.03.2014 (DOY 20–83), during which 62 days were analyzed. The structure was a 12-span naturally ventilated greenhouse with dimensions of $125 \times 80\,\mathrm{m}^2$ (Figure 1) and 5.5 m height arched gable, equipped with an insect-proof, 50-mesh net on the sidewalls, and impermeable 0.5 mm thick polyethylene plastic roof. Tomato (LA–JULIE) (A. B. Zeraim, Inc. Israel) was planted on the 6th of September 2013, upon rows 0.60 m wide, separated 1.8 m apart, with plant density of $0.9\ \mathrm{plants \cdot m^{-2}}$. Plant height during the measurements period varied between 1.3 and 1.8 m, depending on the trellis management and plant pruning. Plants were irrigated

Table 1: Instruments, their heights, and normalized heights in the 3 campaigns.

Measurement	Instrument	Model and manufacturer	Campaign		
			S1; z (m) (Z_S)	S2a **(b)**; z (m) (Z_S)	S3; z (m) (Z_S)
3D wind components, sonic temperature	3D sonic anemometer	CSAT3 Campbell Scientific	4.5 (0.48)	5 **(3)** (1.62)	2.5 (0.58)
H_2O concentration	IRGA	LI-7500 LI-COR	4.5 (0.48)	5 **(3)** (1.62)	2.5 (0.58)
Net radiation	Net radiometer	Q*7.1 REBS	4.9 (0.69)	5 **(3)** (1.24)	2.3 (0.54)
Soil heat flux	Thermopile	HF-3.1 REBS	−0.08 (NA)	−0.08 (NA)	−0.08 (NA)
Soil temperature	Thermocouple	T type, 24 gauge	−0.02 and −0.06 (NA)	−0.02 and −0.06 (NA)	−0.02 and −0.06 (NA)

following regional recommendations for greenhouse tomato. Before plantation, the farmer added compost to the soil (60 $m^3 \cdot Ha^{-1}$). Soil comprised 39% clay, 29% sand, 29% silt, and 3% organic matter. Hence, dry and volumetric soil heat capacities were $C_d = 0.88\ J \cdot g^{-1} \cdot K^{-1}$ and $C_V = 2.05\ MJ \cdot m^{-3} \cdot K^{-1}$ [25].

3.2. Sensors and Data Acquisition. Table 1 presents the instruments, their heights above soil, z, and normalized height, Z_S, in the three campaigns. For S2, the table shows the heights of EC system and net radiometer above (S2a) and below (S2b) the screen. Figure 1 depicts the geometry of each structure and the position of the EC tower and FV miniature thermocouples in each of the structures.

Miniature thermocouples were placed on the same tower of the EC system, at 9 heights ranging from 1 to 5.8 m and from 1.9 to 5.4 m, in S1 and S2, respectively ($-1.34 \le Z_S \le 1.15$ and $0.14 \le Z_S \le 1.83$, resp.), and at 5 heights ranging from 1.5 to 3.8 m in S3 ($0.35 \le Z_S \le 0.89$). All high-frequency data were recorded on a CR3000 data logger (Campbell Scientific Inc., USA).

3.2.1. Eddy Covariance. In S1, the eddy-covariance (EC) system was deployed below the screen at a height of 4.5 m on one of the screenhouse-supporting poles (Figure 1). This position allowed a minimum fetch of about 200 m for the prevailing wind direction in the site. The height of the EC system was between 2.1 and 2.5 m above plant zero-plane displacement height, as estimated according to Stanhill [27] assuming neutral stability. Hence, the height/fetch ratio of the EC system was 1/95–1/80, suitable for surface flux measurements based on footprint models developed for open canopies [28, 29]. A similar EC setup in screenhouses that are similar to S1 had already been reported to be valid by Tanny et al. [3, 12]. In S2, the EC system was deployed on the southeast side of the screenhouse at a height of 5 m, which was 1.3 m above the 50-mesh screen (campaign S2a). In a screenhouse similar to S2, the zero-plane displacement of a canopy-screenhouse system was, for neutral stability, about 0.8 of the screen height [30]. In S2, the prevailing wind was north-northwest, and resulting fetch was about 100 m. Thus, the height/fetch ratio at S2 was about 1/50, which is larger than in S1 but still suitable for surface flux measurements according to simplified footprint models [28]. In S2, an internal EC system was also deployed below the screen (designated as S2b) and above the plants, at a height of 3 m above the ground. Three additional ultrasonic anemometers (CSAT3) were deployed in S2 at heights 1.15, 1.7, and 2.5 m above the ground and below the screen.

In S3, the EC system was deployed on the southeast region of the greenhouse at a height of 2.5 m, which was 2 m below the gable. The zero-plane displacement height of a canopy-greenhouse system was estimated, for neutral stability, to be about 0.67 of the plant height. The dominant wind was north-northwest where the fetch was about 100 m. Thus, the height/fetch ratio at S3 was 1/75–1/60, which is still suitable for surface flux measurement according to simplified footprint models [28].

Data regarding footprint distribution in the three campaigns are given in Table 4 (Section 4.1), which describes data quality analysis.

3.2.2. Flux Variance. For FV analysis, air temperature was measured at 10 Hz by fine-wire miniature thermocouples. Radiation load on thermocouples can introduce small errors; however, due to the small size of the thermocouple junctions and low-radiation load (due to the screen or plastic cover), the errors are assumed negligible [31].

In S1, T-type fTcs (fine-wire thermocouples) were self-constructed in our lab using fine wires of 50 or 76 μm in diameter. When installed in the field, the junction and additional 0.02 m of wire were exposed to the air. In S2 and S3, commercial T-type fTcs (model COCO-002, Omega Engineering Inc., UK), 50 μm in diameter, were installed. Length of exposed wire varied between 0.01 and 0.02 m. In all campaigns, the TC junction was directed upwind and extension wires of 24 gauge SLE thermocouples were used to connect the fTcs to the data logger.

3.2.3. Additional Measurements. In all campaigns, additional measurements (Table 1) were conducted to enable energy balance closure and data analysis. These included net radiation, soil heat flux, and soil temperature. Soil heat flux and storage were measured and calculated following Tanny et al. [3]. Data of these sensors were recorded on a CR23X data logger (Campbell Scientific Inc., USA).

3.3. Data Processing. Eddy-covariance calculations of sensible and latent heat fluxes were done using the EddyPro software (LI-COR, Inc.) which incorporates all necessary raw data filtering and corrections. Quality control of the EC

data was implemented using the common criteria for testing the developed turbulence and steady-state conditions [15].

The developed turbulence criterion is quantified by the value of the integral turbulence characteristic, ITCσ [15]:

$$\mathrm{ITC}\sigma = \left| \frac{(\sigma_x/x_*)_{\mathrm{model}} - (\sigma_x/x_*)_{\mathrm{measurement}}}{(\sigma_x/x_*)_{\mathrm{model}}} \right|, \quad (5)$$

where σ_x is the standard deviation of the variable x and x_* is its dynamical parameter (e.g., u_* for the velocity). The steady-state test is estimated by

$$\mathrm{RN}x = \left| \frac{\left[\overline{w'x'}\right]_{\mathrm{SI}} - \left[\overline{w'x'}\right]_{\mathrm{WI}}}{\left[\overline{w'x'}\right]_{\mathrm{WI}}} \right|, \quad (6)$$

where x' is the scalar of interest, the subscript SI represents the covariance calculated during a short time interval (e.g., 5 min), and the subscript WI is the covariance calculated during the whole averaging interval (30 min).

Using this approach each half hour is categorized according to one of three quality levels from high to low. Highest quality data (classes 1–3) can be used for fundamental research and development of parametrizations (ITCσ, RNx < 0.5), intermediate quality data (classes 4–6) can be used for general use like routine flux measurements (0.51 < ITCσ, RNx < 2.5), and lowest quality data (classes 7–9) can be used for orientation only or rejected [15]. Since in the present study the EC data were used as a reference for flux measurements of sensible and latent heat fluxes, data up to class 6, representing the intermediate category of "routine flux measurements," were chosen for analysis.

For the FV data analysis, sensible heat flux was calculated by (4) based on the half-hourly standard deviation of the temperature measured by each fTc. All measurements by the miniature fTcs were conducted at 10 Hz; nevertheless, data were also analyzed at lower frequencies of 1, 2, and 5 Hz. Lower frequency analysis was done by skipping the corresponding data at the temperature time series. This analysis was performed to examine the possibility of measurements at sampling rates lower than 10 Hz, with the goal of using low-cost data acquisition systems in future application of the FV technique.

Data of each campaign were divided into two periods: calibration and validation, as described in Table 2. This division was chosen so as to simulate future application of the FV method, where simultaneous FV and EC data from the initial period are used for calibrating the system, while, during the consecutive period, the FV is operated independently. Hence, during calibration the corresponding value of C_T was extracted from regressions of H_{FV} from (4), against direct eddy-covariance measurements of sensible heat flux, H_{EC}. The value of C_T thus obtained was then used along with σ_T from the temperature measurements in the validation phase for estimating H_{FV} using (4).

Data were also categorized according to the atmospheric stability conditions within each of the structures using the value of L, the Obukhov length scale (1), to indicate the stability level. The criteria based on Webb [32], summarized in Table 3, were adopted in the present analysis.

Table 2: Calibration and validation periods of the three campaigns.

Experiment	Calibration period (DOY)	Validation period (DOY)
S1 (2011)	219–230 (11 days)	231–241 (10 days)
S2 (2013)	133–145 (13 days)	146–166 (21 days)
S3 (2014)	20–49 (29 days)	50–83 (33 days)

Table 3: Stability regimes and corresponding values of L.

Stability	L
Stable	$0 < L < 200$
Neutral	$\lvert L\rvert > 200$
Unstable	$-200 < L < 0$

4. Results

4.1. Quality Control of EC Data. Figure 2 shows the percentage of EC data points within each range of quality levels: 1–3 (research), 4–6 (flux data), and 7–9 (orientation). Figures 2(a) and 2(b) show the results for the steady-state test of the covariances, $w'T'$ and $w'q'$, that are proportional to the sensible and latent heat fluxes, respectively. Figures 2(c) and 2(d) show the results of developed turbulence tests for the horizontal and vertical velocity components, u and w, and Figures 2(e) and 2(f) for the temperature and absolute humidity, T and q, respectively. In the analysis, data from S2 were presented separately for measurements below (S2b) and above (S2a) the screen. Figure 2 shows that, for most variables, the percentage of data points with flags 7–9 is relatively low. This indicates that most data points in the three structures met the quality criteria of developed turbulence and steady state.

Table 4 summarizes the data quality results. Data points under neutral and stable conditions were excluded from further analysis in this paper. Hence, results in subsequent sections of this paper are based on data that met the three quality criteria: unstable conditions, quality flag <7, and footprint peak within the structure under study.

One of the basic assumptions of the eddy-covariance technique is that measurements are done within the constant-flux layer, namely, the vertical flux of the measured scalar is constant with height. This assumption was examined in campaign S2 where 4 ultrasonic anemometers were installed below the screen and one above it. Figure 3 shows the vertical distribution of mean friction velocity, which represents the vertical flux of horizontal momentum, measured during S2. Figure 3 clearly shows that under the screen and above the plants, at z (Z_{S}) = 1.7 (0.05), 2.45 (0.39), and 3 m (0.64), the friction velocity is nearly constant with height, supporting the constant-flux layer assumption. Above the screen (Z_{S} = 1.55), the friction velocity is much higher. This is presumably due to the screen being a sink of momentum due to drag. A similar change in friction velocity across a shading screen was observed by Tanny et al. [13].

4.2. Energy Balance Closure. Figure 4 presents the regressions of half-hourly values of consumed energy ($LE + H$) versus available energy ($Rn - G$) in each of the campaigns. Equations

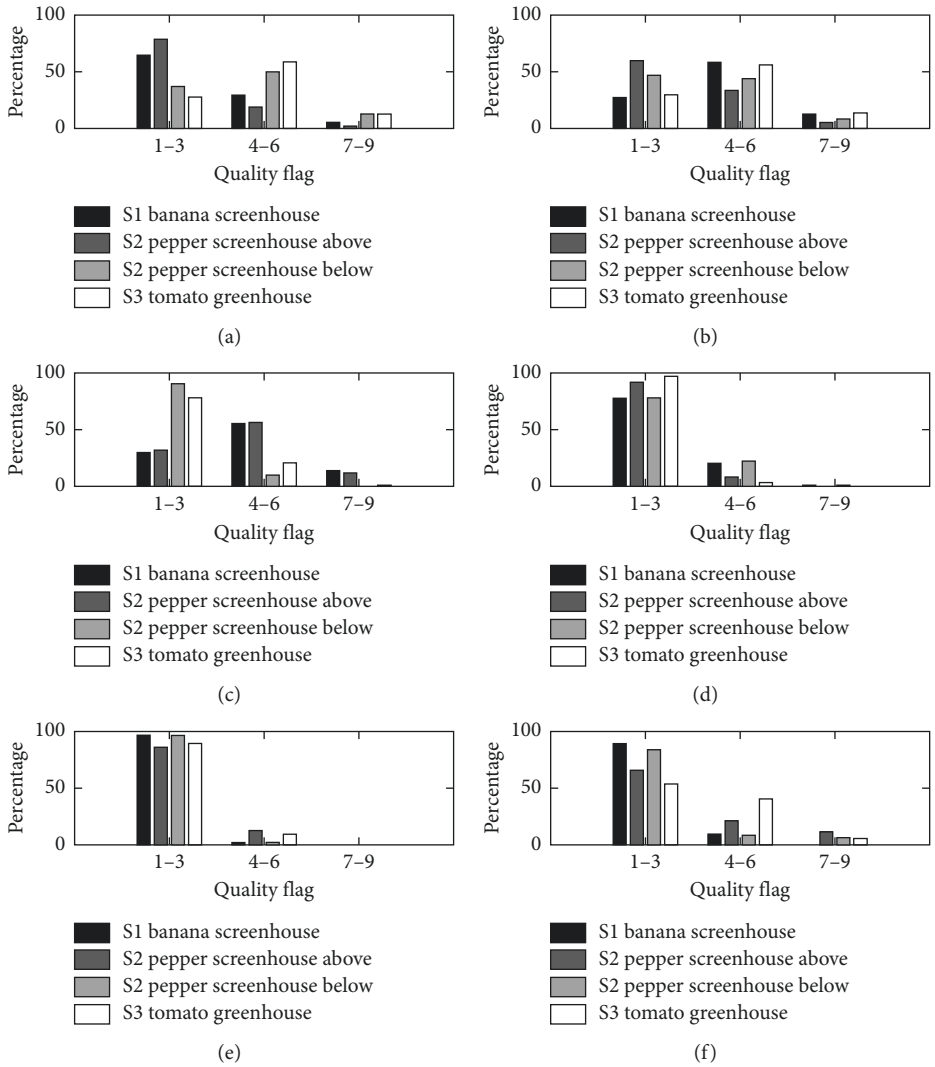

Figure 2: Results of quality control tests: the percentage of data points within each range of quality category: 1–3 (research), 4–6 (flux data), and 7–9 (orientation). (a) Steady-state test: Cov $(w'T')$; (b) steady-state test: Cov $(w'q')$; (c)ITC$\sigma(u)$; (d)ITC$\sigma(w)$; (e)ITC$\sigma(T)$; (f)ITC$\sigma(q)$.

Table 4: Summary of data quality control.

	Year	Total data points	Stable	Neutral	Unstable	Flags 1–6	Footprint peak within structure (%)
S1	2011	1103	405	68	630	501	97
S2 above	2013	1171	338	165	668	573	95
S2 below	2013	2347	1795	38	514	396	99
S3	2014	4645	1822	219	2604	2509	100

Columns from left to right represent campaign code, year, total number of available data points, number of data points under stable conditions, number of data points under neutral conditions, number of data points under unstable conditions, number of data points with quality flags 1–6, and percentage of data points whose flux footprint peak is within the structure.

(7)–(10) below present the linear fits for the energy balance closure analyses in Figure 4.

The results show that, for S1, energy balance slope was low (0.41); however, the high R^2 indicates close correlate between consumed $(LE + H)$ and available $(Rn - G)$ energy. For S2a (pepper screenhouse above the screen), both slope and R^2 were reasonable. For S2b (pepper screenhouse below the screen) and S3, low closure slopes and very low values of R^2 were obtained.

$$\text{S1}: \quad LE + H = 0.41(Rn - G), \quad R^2 = 0.91, \tag{7}$$

$$\text{S2a}: \quad LE + H = 0.76(Rn - G), \quad R^2 = 0.66, \tag{8}$$

$$\text{S2b}: \quad LE + H = 0.53(Rn - G), \quad R^2 = 0.17, \tag{9}$$

$$\text{S3}: \quad LE + H = 0.39(Rn - G), \quad R^2 = 0.29. \tag{10}$$

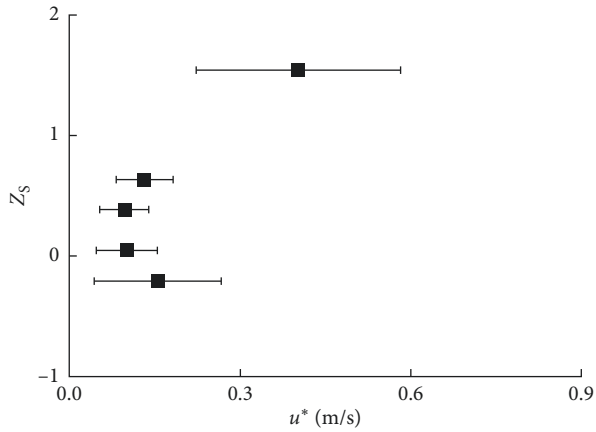

Figure 3: Vertical distribution of the half-hourly friction velocity averaged during campaign S2. Horizontal lines represent the standard error. Canopy height is $Z_S = 0$. Screen height is $Z_S = 1$.

Due to the poor R^2 values of the energy balance closure of S2b and S3, the subsequent analyses of this paper were conducted only for campaigns S1 and S2a.

4.3. Sensible Heat Flux: FV Method

4.3.1. FV Analysis Based on Temperature Signal of the Ultrasonic Anemometer. The FV method was initially applied by analyzing the temperature signal measured by the ultrasonic anemometers (CSAT3, Campbell Scientific Inc., USA). The sensible heat flux was estimated by (4) where during the calibration, the constant C_T was estimated from the slope of the regression between H_{FV} and H_{EC}. For validation, the constant C_T obtained during calibration was used to estimate H_{FV} that was eventually compared with H_{EC}. Figure 5 shows the regressions obtained during calibration and validation in the two campaigns, S1 and S2a.

The statistical variables associated with the regressions in Figure 5 are given in Table 5. The results in both Figure 5 and Table 5 show that good correlation was obtained between the two fluxes in campaigns S1 and S2a.

4.3.2. FV Analysis Based on Temperature Signal of the Miniature Thermocouples. In order to develop a simple measurement system for estimating the sensible heat flux by the FV technique, analysis was carried out for the data of the thermocouples installed at the different heights. For each sensor, a regression was calculated between H_{FV} and H_{EC}, and an optimal C_T value was determined, which guaranteed a regression slope closest to one. Figure 6 shows vertical distributions of R^2 and C_T as a function of normalized height during calibration and validation in the two campaigns.

The results in Figure 6 show that, in S1 (Figure 6(a)), the value of R^2 decreased with height from within the canopy and up to the canopy top, and then, it increases towards the screen level. A slight reduction in R^2 is observed above the screen. In S2 (Figure 6(c)), R^2 was nearly constant just above the canopy and increased sharply near the screen. Maximum R^2 during calibration was obtained in S1 at $z = 6$ m ($Z_S = 1.41$) and in S2 at $z = 5$ m ($Z_S = 1.54$). In both campaigns, the C_T value generally increased with height and reached a maximum value just above the screen.

Table 6 shows statistical variables and C_T values for the calibration and validation periods in campaigns S1 and S2a, for the miniature thermocouple that provided the best R^2 in each campaign, as deduced from Figure 6.

Farmers, who will apply the FV method, are not expected to use high frequency (10 Hz) measurements that require expensive data loggers, as done in this study. More probably, simple data acquisition systems with lower sampling frequency would be more practical for such purposes. Therefore, an attempt was made to examine the performance of the FV technique under sampling frequencies lower than 10 Hz. Hence, the standard deviation of the temperature signal was analyzed at frequencies of 5, 2, 1, 0.5, 0.1, and 0.0166 Hz. The analysis was done for the fTc at $z = 5$ m height ($Z_S = 1.54$) in S2a which provided the best R^2 at 10 Hz data analysis (Figure 6). Figure 7 shows relations between characteristics of regressions between H_{FV} and H_{EC}, when H_{FV} is calculated by each of the lower frequencies, to that obtained at 10 Hz.

It is shown that ratios between all regression parameters, namely, R^2 (Figure 7(a)), slope (Figure 7(b)), and intercept (Figure 7(c)) are unaffected by reducing the data analysis frequency down to 0.5 Hz (i.e., one sample every 2 s!). This result implies that data acquisition systems of relatively low sampling rates (and presumably lower price) can be used in future implementation of the FV technique for day-to-day use by farmers.

4.4. Latent Heat Flux: FV Method. The flux-variance latent heat flux was estimated in each campaign, S1 and S2a, assuming a closed energy balance closure and using H_{FV}. Figure 8 presents the regressions between latent heat flux estimated by the FV technique, LE_{FV}, and LE_{EB} deduced by forcing energy balance closure using H_{EC}. The corresponding coefficients of the regressions are given in Table 7. Results show high capability of the FV method in estimating the latent heat flux in the two campaigns with deviations of up to 8% (calibration period of S2a) between measured and estimated latent heat flux.

5. Discussion

This is the first study that examines the applicability of the flux-variance method in protected environments like screenhouses and greenhouses. The flux-variance method is based on MOST (Section 2), which assumes steady state and well-developed turbulence conditions. In campaign S1 (the banana screenhouse), best performance of the FV method, with largest R^2, was realized within the canopy and above the screen (Figure 6(a)). The performance was lowest just below the canopy top. In a banana plantation, the leaf area density is low near the ground, increases with height, and then decreases again at plants' top [8]. The regions of high R^2 (Figure 6(a)) are commensurate with regions where leaf area

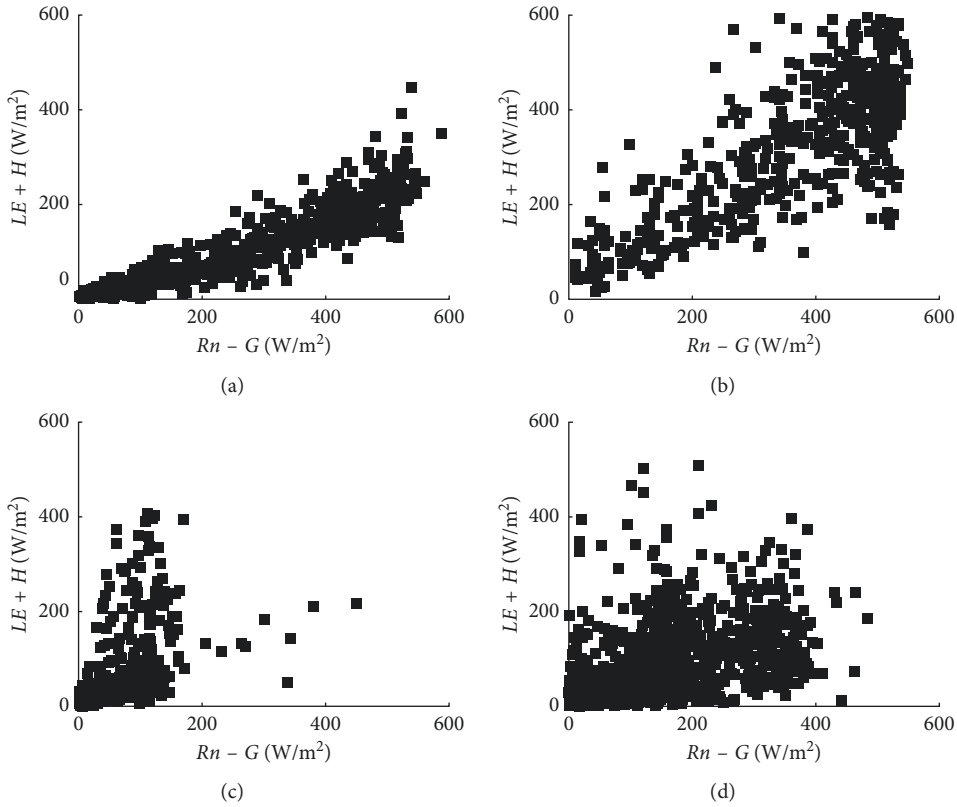

Figure 4: Energy balance closure analyses for the three campaigns. Each symbol represents a measured half-hourly data point. (a) S1: banana screenhouse; (b) S2: pepper screenhouse (above screen); (c) S2: pepper screenhouse (below screen); (d) S3: tomato greenhouse.

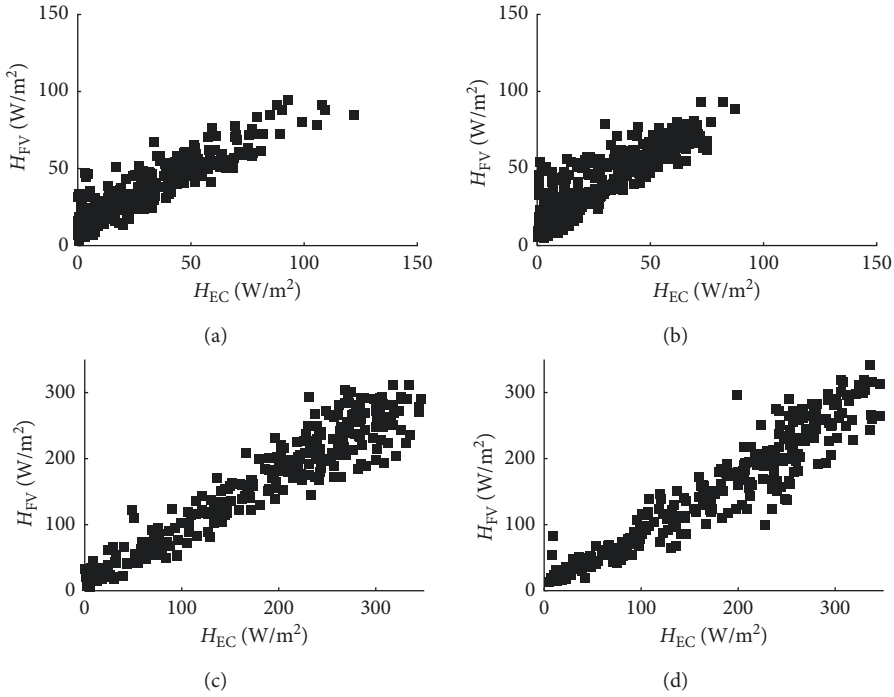

Figure 5: Sensible heat flux measured by EC versus that estimated by FV for calibration and validation during the two campaigns. FV data are calculated based on the temperature signal of the ultrasonic anemometer. S1 banana screenhouse: (a) calibration; (b) validation. S2 pepper screenhouse (above screen): (c) calibration; (d) validation.

Table 5: Statistical variables and C_T value for the regressions between sensible heat flux measured by the EC and estimated by FV.

		DOY	C_T	Slope, a	RMSE (W·m^{-2})	R^2
S1 banana 2011	Calibration	219–230	1.98	0.99	12.68	0.70
	Validation	231–241	1.98	1.03	13.91	0.85
S2a pepper 2013	Calibration	133–145	1.51	0.98	23.45	0.88
	Validation	146–166	1.51	1.01	24.18	0.91

FV data are based on the temperature signal of the ultrasonic anemometer. The results correspond to the graphs in Figure 5.

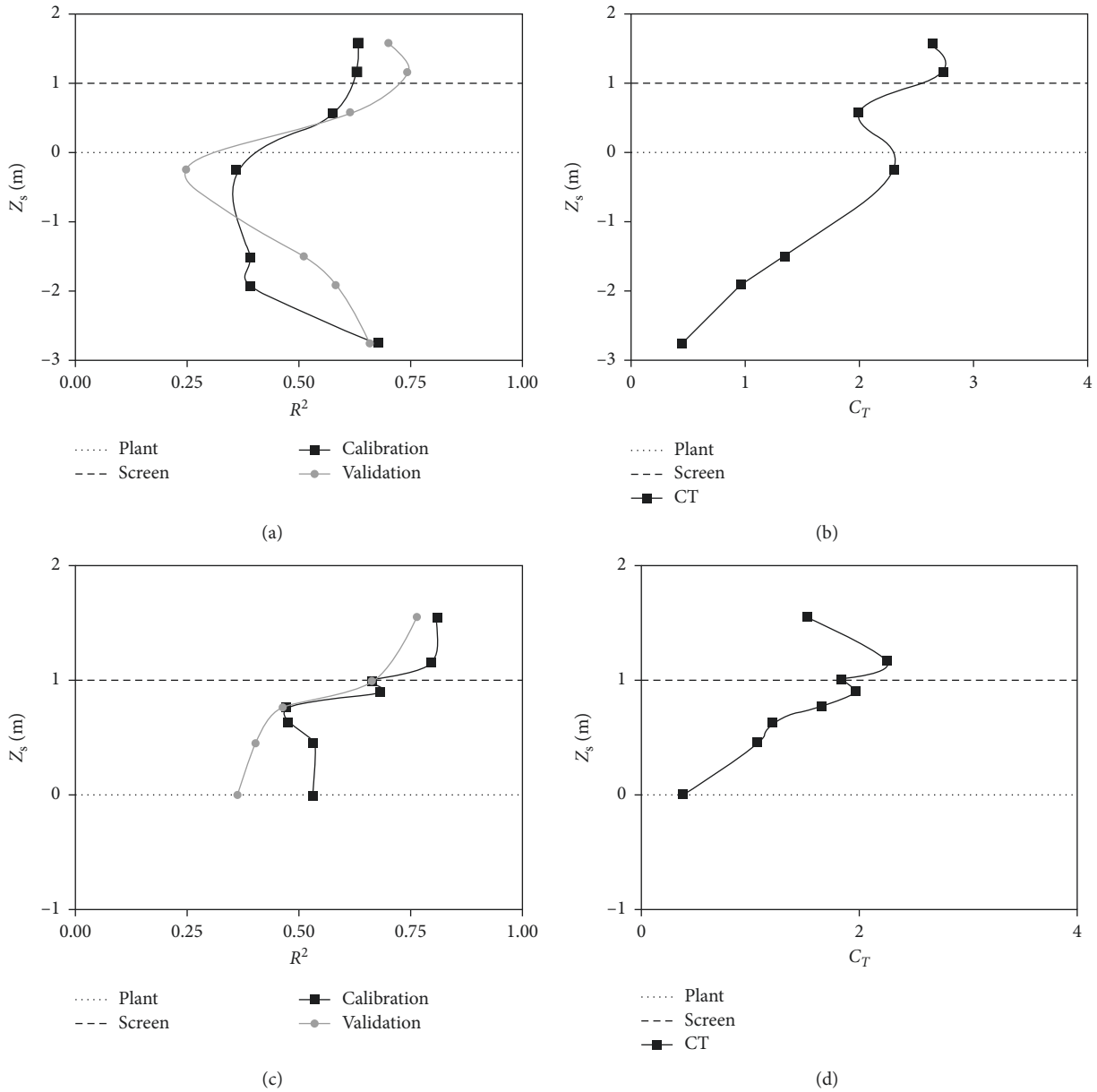

Figure 6: Vertical distributions of R^2 during calibration (black line) and validation (grey line) in the two campaigns, S1 (a) and S2 (c), respectively. (b) and (d) are the corresponding distributions of C_T for the validation conditions. In S2, calibration and validation were against reference measurements of H_{EC} above the screen. $Z_S = 0$, canopy top; $Z_S = 1$ screen height.

density is low, presumably since, in these regions, MOST is less violated by the high density of canopy elements. In the pepper screenhouse (Figure 6(c)), R^2 which represents the performance of the FV method increases with height from plants' tops towards the screen and reaches its maximum above the screen. This distribution may also be related to the fact that MOST validity is higher above the screen where conditions of well-developed turbulence are more favorable.

Table 6: Statistical variables and C_T value for the regressions between sensible heat fluxes measured by the EC and FV methods.

		DOY	C_T	Slope, a	RMSE (W·m^{-2})	R^2
S1 banana 2011	Calibration	219–230	2.64	0.99	8.38	0.82
	Validation	231–241	2.64	1.02	8.56	0.85
S2a pepper 2013	Calibration	133–145	1.52	1.01	26.78	0.9
	Validation	146–166	1.52	1.03	31.92	0.87

Results are presented for the miniature thermocouple positioned at the height that provided the best performance in each campaign.

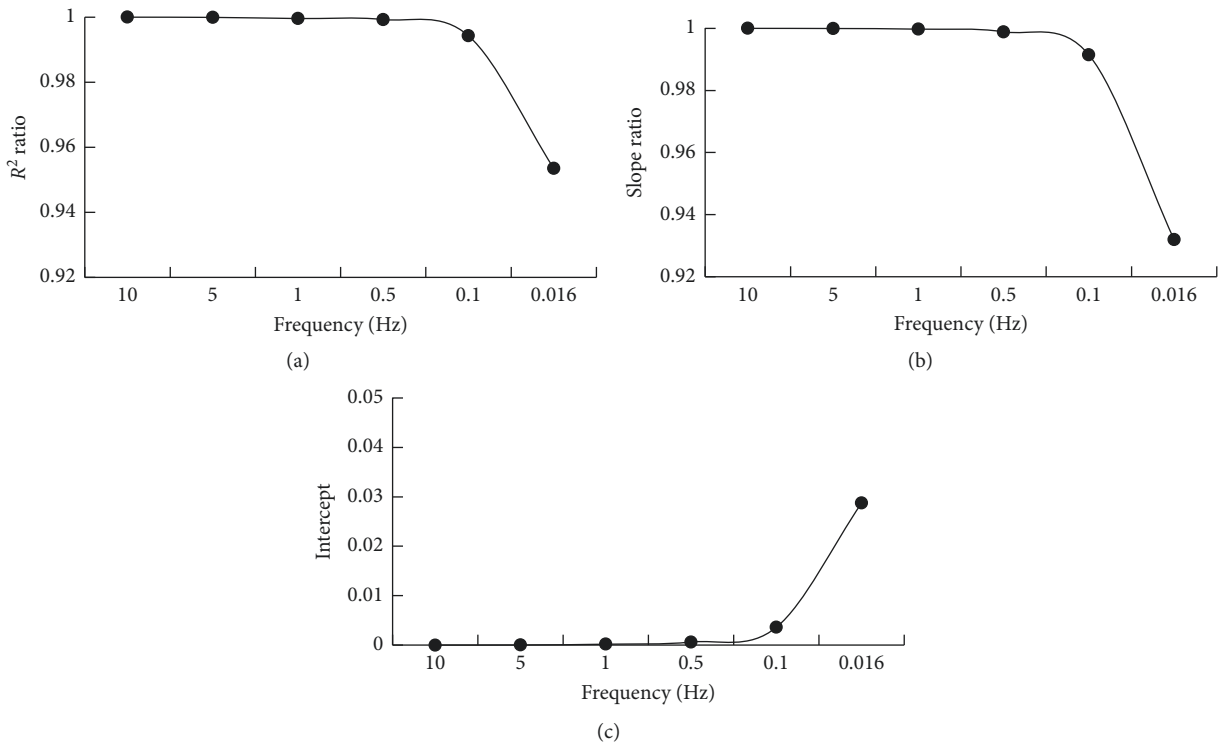

Figure 7: Ratio between the regression R^2, slope, and the difference between intercept, between H_{FV} and H_{EC}, of data analysis at each frequency to those obtained at 10 Hz. (a) Coefficient of determination; (b) slope; (c) Y-axis intercept difference.

The three structures examined in this study are very popular among growers in mild winter climates where water scarcity is constantly increasing, and modified environments are widely used by growers to increase water saving. Hence, whole canopy evapotranspiration measurements are essential for improving the irrigation management. Although the use of the EC technique has already been established in various types of screenhouses (e.g., [2, 3, 13]), to the best of our knowledge, this is the first study which examined the use of the EC method to measure turbulent fluxes in a naturally ventilated greenhouse (S3) with an impermeable plastic roof. Therefore, one of the goals of this study was to determine and compare the quality of data used for the EC analysis in the different structures.

Screenhouses allow relatively intense interaction between inside and outside through the permeable roof, as was already presented by Tanny et al. [3] for a banana crop under a light-shading screen. On the contrary, the greenhouse has an impermeable roof, which totally blocks any such interaction, as well as the vertical exchange of mass between the plants and the outside atmosphere. However, the greenhouse investigated in S3 had screened sidewalls that allowed natural ventilation by horizontal wind flow over the tomato plants. This wind flow facilitated the development of the turbulent canopy flow as was illustrated by the reasonable results of the quality tests of ITCσ and RNx in the greenhouse (Table 4), also for the temperature, humidity, and vertical velocity fluctuations (Figure 2). On the other hand, the impermeable plastic roof restricted the vertical flux of momentum, mass, and heat, thereby inducing significant advective effects in the greenhouse, which significantly deteriorated the energy balance closure and R^2 (10). In a similar manner, the dense insect-proof screen in campaign S2b also restricted the vertical fluxes, which resulted with a poor energy balance closure slope and R^2 values (9).

This observation suggests that, in greenhouses, the validity of the two common data quality criteria of developed turbulence and steady state is insufficient to guarantee reliable EC flux measurements. Conditions of developed

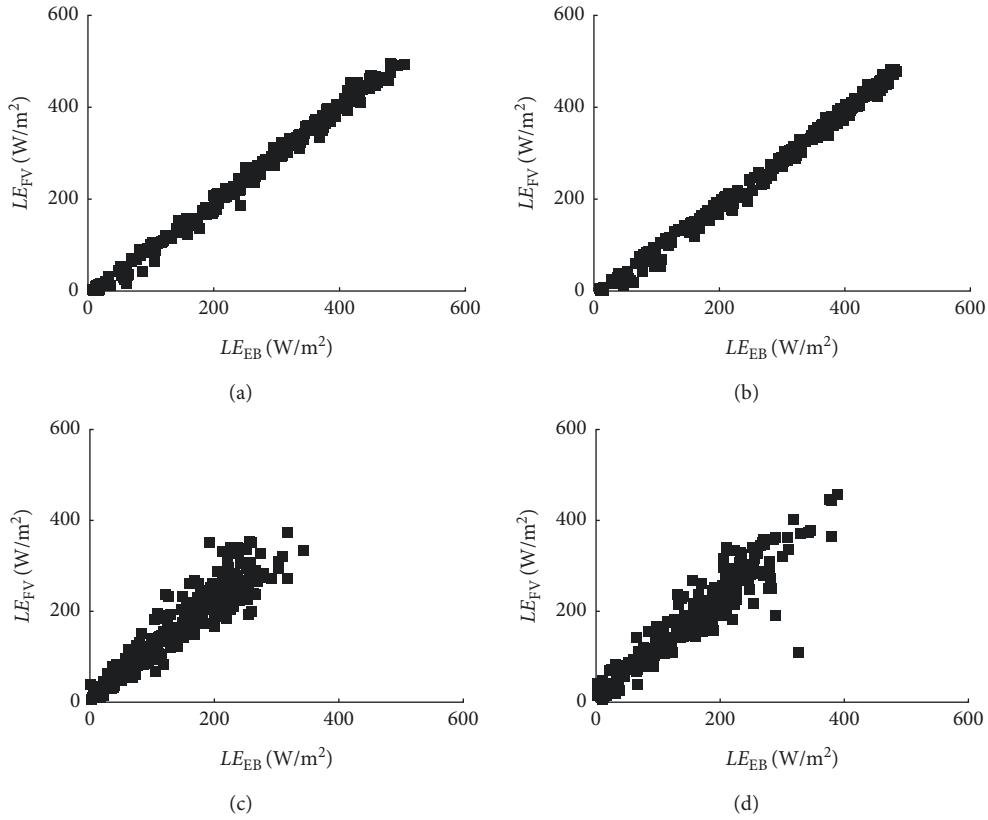

Figure 8: The latent heat flux estimated based on FV technique, LE_{FV}, versus the one estimated by forcing the energy balance closure, LE_{EB}. S1 banana screenhouse: (a) calibration; (b) validation. S2 pepper screenhouse (above screen): (c) calibration; (d) validation. Statistical data of these graphs are presented in Table 7.

Table 7: Statistical variables for the regressions between latent heat fluxes deduced from energy balance and estimated by the FV method (Figure 8).

		DOY	Slope, a	Intercept, b	RMSE (W·m^{-2})	R^2
S1 banana 2011	Calibration	219–230	1.02	−12.96	10.32	0.99
	Validation	231–241	1.01	−16.09	8.96	0.99
S2a pepper 2013	Calibration	133–145	1.08	9.02	32.39	0.93
	Validation	146–166	1.07	11.67	33.64	0.92

Results are presented for the thermocouple positioned at the measurement height that provided the best performance in each campaign.

turbulent flow and steady state can prevail in naturally ventilated greenhouses even when the scalars are eventually advected horizontally due to the impermeable roof of the greenhouse. Detailed advection measurements require the deployment of several EC systems at different downwind locations, a task that was outside the scope of the present study.

6. Conclusions

A field experiment was carried out in 3 different naturally ventilated agricultural structures, two screenhouses, and a greenhouse to study the suitability of a simple turbulent transport technique, namely, the flux variance, in estimating sensible and latent heat fluxes. The major conclusions of this study are as follows: (i) Quality control analysis of the EC method showed that conditions in the shading and insect-proof screenhouses (above the screen) were reasonable for flux measurements. However, in the plastic-covered greenhouse and in the insect-proof screenhouse below the screen, energy balance closure and its R^2 were poor. Therefore, the FV method could not be employed in these campaigns; (ii) The FV technique was suitable for reliable estimates of H and LE in shading and insect-proof screenhouses, provided the miniature temperature sensors are positioned above the screen; and (iii) data analysis frequency of the temperature signal used in the FV analysis could be reduced down to 0.5 Hz with no effect on the statistical parameters of the regressions between sensible heat flux measured by EC and estimated by FV. Hence, for the future application of this method, simple and low-cost temperature sensors and data acquisition systems can be used effectively.

Nomenclature

C_T: A similarity constant (–)
c_p: Air specific heat at constant pressure ($J \cdot kg^{-1} \cdot K^{-1}$)
d: Zero-plane displacement height (m)
g: Gravitational acceleration ($m \cdot s^{-2}$)
h_c: Canopy height (m)
h_s: Roof height, either screen (S1 and S2) or plastic (S3) (m)
H: Sensible heat flux ($W \cdot m^{-2}$)
H_{EC}: Sensible heat flux measured by eddy covariance ($W \cdot m^{-2}$)
H_{FV}: Sensible heat flux estimated by flux variance ($W \cdot m^{-2}$)
k: von-Karman's constant (–) (=0.41)
L: Obukhov length scale (m) (1)
LE: Latent heat flux ($W \cdot m^{-2}$)
LE_{FV}: Latent heat flux deduced from flux variance ($W \cdot m^{-2}$)
LE_{EB}: Latent heat flux deduced by forcing the energy balance closure ($W \cdot m^{-2}$)
T: Air temperature (°C)
T_*: Temperature-scaling parameter, $T_* = \langle w'T' \rangle / u_*$ (°C)
T': Air temperature fluctuations (°C)
U: Horizontal mean air velocity ($m \cdot s^{-1}$)
u_*: Friction velocity ($m \cdot s^{-1}$)
u', w': Horizontal and vertical velocity fluctuations ($m \cdot s^{-1}$)
Z: Measurement height (m)
Z_S: $(z\text{-}h_c)/(h_s\text{-}h_c)$ normalized measurement height (–).
ζ: Atmospheric stability parameter, $(z - d)/L$ (–)
ρ: Air density ($kg \cdot m^{-3}$)
σ_T: Standard deviation of air temperature (°C)
EC: Eddy covariance
fTc: Fine-wire thermocouple
FV: Flux variance
S1: Measurements campaign in the banana screenhouse with 8% shading screen
S2: Measurements campaign in the pepper screenhouse covered with a 50-mesh insect-proof screen
S2a: Measurements above the screen during S2
S2b: Measurements below the screen during S2
S3: Measurements campaign in the tomato greenhouse with a plastic roof.

Conflicts of Interest

The authors declare that they have no conflicts of interest.

Acknowledgments

The authors thank Mr. Victor Lukyanov for technical help. The authors also thank Professor Gabriel Katul for his helpful suggestions. This research was supported by Research Grant Award no. IS-4374-11C from BARD, the United States–Israel Binational Agricultural Research and Development Fund, and the Chief Scientist of the Israeli Ministry of Agriculture under Grant no. 304-0444.

References

[1] M. Teitel, O. Liran, J. Tanny, and M. Barak, "Wind driven ventilation of a mono-span greenhouse with a rose crop and continuous screened side vents and its effect on flow patterns and microclimate," *Biosystems Engineering*, vol. 101, no. 1, pp. 111–122, 2008.

[2] M. Moeller, J. Tanny, Y. Li, and S. Cohen, "Measuring and predicting evapotranspiration in an insect-proof screenhouse," *Agricultural and Forest Meteorology*, vol. 127, no. 1-2, pp. 35–51, 2004.

[3] J. Tanny, L. Haijun, and S. Cohen, "Airflow characteristics, energy balance and eddy covariance measurements in a banana screenhouse," *Agricultural and Forest Meteorology*, vol. 139, no. 1-2, pp. 105–118, 2006.

[4] C. von Zabeltitz, *Integrated Greenhouse Systems for Mild Climates : Climate Conditions, Design, Construction, Maintenance, Climate Control*, Springer-Verlag, Berlin, Heidelberg, Germany, 2011.

[5] N. Gruda and J. Tanny, "Protected crops-recent advances, innovative technologies and future challenges," *Acta Horticulturae*, vol. 1107, pp. 271–277, 2015.

[6] E. Kitta, A. D. Baille, N. Katsoulas, N. Rigakis, and M. M. Gonzalez-Real, "Effects of cover optical properties on screenhouse radiative environment and sweet pepper productivity," *Biosystems Engineering*, vol. 122, pp. 115–126, 2014.

[7] C. Kittas, N. Katsoulas, N. Rigakis, T. Bartzanas, and E. Kitta, "Effects on microclimate, crop production and quality of a tomato crop grown under shade nets," *Journal of Horticultural Science and Biotechnology*, vol. 87, no. 1, pp. 7–12, 2012.

[8] M. B. Siqueira, G. G. Katul, and J. Tanny, "The effect of the screen on the mass, momentum, and energy exchange rates of a uniform crop situated in an extensive screenhouse," *Boundary-Layer Meteorology*, vol. 142, no. 3, pp. 339–363, 2012.

[9] U. Dicken, S. Cohen, and J. Tanny, "Effect of plant development on turbulent fluxes of a screenhouse banana plantation," *Irrigation Science*, vol. 31, no. 4, pp. 701–713, 2013.

[10] E. Kitta, A. Baille, N. Katsoulas, and N. Rigakis, "Predicting reference evapotranspiration for screenhouse-grown crops," *Agricultural Water Management*, vol. 143, pp. 122–130, 2014.

[11] M. Pirkner, U. Dicken, and J. Tanny, "Penman-Monteith approaches for estimating crop evapotranspiration in screenhouses-a case study with table-grape," *International Journal of Biometeorology*, vol. 58, no. 5, pp. 725–737, 2014.

[12] J. Tanny, U. Dicken, and S. Cohen, "Vertical variation in turbulence statistics and energy balance in a banana screenhouse," *Biosystems Engineering*, vol. 106, no. 2, pp. 175–187, 2010.

[13] J. Tanny, V. Lukyanov, M. Neiman, S. Cohen, M. Teitel, and I. Seginer, "Energy balance and partitioning and vertical profiles of turbulence characteristics during initial growth of a banana plantation in a screenhouse," *Agricultural and Forest Meteorology*, vol. 256-257, pp. 53–60, 2018.

[14] M. Aubinet, T. Vesala, and D. Papale, *Eddy Covariance : a Practical Guide to Measurement and Data Analysis*, Springer, Dordrecht, Netherlands, 2012.

[15] T. Foken, R. Leuning, S. R. Oncley, M. Mauder, and M. Aubinet, "Corrections and data quality control," in *Eddy Covariance*, pp. 85–131, Springer, Dordrecht, Netherlands, 2012.

[16] K. H. Wesson, G. Katul, and C.-T. Lai, "Sensible heat flux estimation by flux variance and half-order time derivative methods," *Water Resources Research*, vol. 37, no. 9, pp. 2333–2343, 2001.

[17] H. A. R. De Bruin, W. Kohsiek, and B. J. J. M. Van Den Hurk, "A verification of some methods to determine the fluxes of momentum, sensible heat, and water vapour using standard deviation and structure parameter of scalar meteorological

quantities," *Boundary-Layer Meteorology*, vol. 63, no. 3, pp. 231–257, 1993.

[18] C. I. Hsieh, L. Mei-Chun, H. Yue-Joe, and C. Tsang-Jung, "Estimation of sensible heat, water vapor, and CO2 fluxes using the flux-variance method," *International Journal of Biometeorology*, vol. 52, no. 6, pp. 521–533, 2008.

[19] C.-I. Hsieh, G. G. Katul, J. Schieldge, J. Sigmon, and K. R. Knoerr, "Estimation of momentum and heat fluxes using dissipation and flux-variance methods in the unstable surface layer," *Water Resources Research*, vol. 32, no. 8, pp. 2453–2462, 1996.

[20] G. G. Katul and C. I. Cheng, "A note on the flux-variance similarity relationships for heat and water vapour in the unstable atmospheric surface layer," *Boundary-Layer Meteorology*, vol. 90, no. 2, pp. 327–338, 1999.

[21] J. D. Albertson, M. B. Parlange, G. G. Katul, C.-R. Chu, H. Stricker, and S. Tyler, "Sensible heat flux from arid regions: a simple flux-variance method," *Water Resources Research*, vol. 31, no. 4, pp. 969–973, 1995.

[22] J. C. Wyngaard, O. R. Cot, and Y. Izumi, "Local free convection, similarity, and the budgets of shear stress and heat flux," *Journal of the Atmospheric Sciences*, vol. 28, no. 7, pp. 1171–1182, 1971.

[23] T. E. Twine, W. P. Kustas, J. M. Norman et al., "Correcting eddy-covariance flux underestimates over a grassland," *Agricultural and Forest Meteorology*, vol. 103, no. 3, pp. 279–300, 2000.

[24] Y. Mekhmandarov, M. Pirkner, O. Achiman, and J. Tanny, "Application of the surface renewal technique in two types of screenhouses: sensible heat flux estimates and turbulence characteristics," *Agricultural and Forest Meteorology*, vol. 203, pp. 229–242, 2015.

[25] D. A. DeVries, "Thermal Properties of soils," in *Physics of Plant Environment*, W. R. van Wijk, Ed., pp. 210–235, North-Holland Publishing Co., Amsterdam, Netherlands, 1963.

[26] S. Ravikovitch, *Soils of Israel, Formation and Characteristics of the Soils in Israel*, (in Hebrew), Hakibbutz Hameuchad, Tel-viv, Israel,1981.

[27] G. Stanhill, "A simple instrument for the field measurement of turbulent diffusion flux," *Journal of Applied Meteorology*, vol. 8, no. 4, pp. 509–513, 1969.

[28] C. I. Hsieh, G. Katul, and T. W. Chi, "An approximate analytical model for footprint estimation of scalar fluxes in thermally stratified atmospheric flows," *Advances in Water Resources*, vol. 23, no. 7, pp. 765–772, 2000.

[29] H. P. Schmid, "Experimental design for flux measurements: matching scales of observations and fluxes," *Agricultural and Forest Meteorology*, vol. 87, no. 2-3, pp. 179–200, 1997.

[30] J. Tanny, M. Moeller, and S. Cohen, "Aerodynamic properties of boundary layers along screens," *Biosystems Engineering*, vol. 102, no. 2, pp. 171–179, 2009.

[31] E. Erell, V. Leal, and E. Maldonado, "Measurement of air temperature in the presence of a large radiant flux: an assessment of passively ventilated thermometer screens," *Boundary-Layer Meteorology*, vol. 114, no. 1, pp. 205–231, 2005.

[32] E. K. Webb, "Profile relationships: the log-linear range, and extension to strong stability," *Quarterly Journal of the Royal Meteorological Society*, vol. 96, no. 407, pp. 67–90, 1970.